Automated Region Detection In Near-Infrared Breast Imaging Based Upon Contrast To Noise Ratios

Xiaomei Song[1], Brian W. Pogue[1], Shudong Jiang[1], Hamid Dehghani[1]
Marvin M. Doyley[2], Tor D. Tosteson[3], Steven P. Poplack[4], Keith D. Paulsen[1]
[1]Thayer School of Engineering, Dartmouth College, Hanover NH 03755
[2]Department of Diagnostic Radiology, Dartmouth Medical School, Hanover NH 03755
[3]Biostatistics, Norris Cotton Cancer Center, Dartmouth-Hitchcock Medical Center, Lebanon NH 03756
[4]Deparment of Diagnostic Radiology, Dartmouth-Hitchcock Medical Center, Lebanon NH 03756

ABSTRACT

The Contrast to Noise Ratio (CNR) was used as the criterion to automatically segment out regions of interest (ROI) within near-infrared optical images. CNR is defined as the relative difference between the average property values within the ROI and those within background region, divided by the average variation in the background. The goal of this work was to develop a set of tools for assessment of CNR within ROIs associated with regions of high (i) absorption, (ii) scattering, (iii) chromophore concentration or (iv) scattering power. Once the CNR is calculated throughout the image, it is possible to segment out regions based upon this number. The major issues to be resolved in using this approach have been (i) choice of appropriate background area, (ii) choice of ROI size and (iii) ROI location. These three issues were examined in detail in theoretical studies, and then implemented in test studies.

In initial studies, a theoretical assessment was completed, using a fixed amount of noise added to simulated data measurements. From this simulated data images were reconstructed and automated region of interest detection and sampling were achieved. Three methods of choosing the relevant background values were developed to calculate the CNR and construct the contrast-detail curves. The choices of backgrounds were (i) ROIs sampled at the same radial distance in the image, (ii) randomly sampled ROI of the same size as the original, and (iii) all of the available background. Different spatial resolution and contrast resolution were achieved in these 3 methods, and it was concluded that the first approach was the most practical.

In a second part of the study, maximum CNR calculated was used to estimate the position of heterogeneity. Heterogeneities with different location and sizes were used to evaluate the sensitivity of the contrast and size of the heterogeneity to the system accuracy. It was concluded that based upon sampling all possible values of size and location of the ROI, there was a maximal value of CNR near the location and size of the true region which was imaged. To significantly reduce the computation time of finding the maximum CNR, a new method using linear convolution of the image with a test ROI was developed to allow automated ROI detection within a few seconds.

1. INTRODUCTION

The development of Near-Infrared (NIR) diffuse tomography for early detection of breast cancer may provide an effective diagnostic tool to non-invasively quantify oxygen saturation, hemoglobin concentration, water concentration, scattering and potentially exogenous chromophores [1-12]. Tumors tend to have a higher level of vascularity due to hyperactive angiogenesis leading to optical contrast to regular issues at the near-infrared spectrum, or light between 650 nm and 900 nm. Detecting these changes with optical absorption and scattering based tomography requires implementation of accurate and fast image reconstruction algorithms. Because the reconstruction process results in moderate resolution images, it is becoming increasingly important to develop tools to accurately interpret the reconstructed image and efficiently find the shape, size and location of the tumor, or the region of interest. In most of current preclinical and clinical NIR tomography studies, the shape and location of the ROI in the reconstructed image is decided by a radiologist projecting what is observed in the x-ray mammograms into the circular tomographic coordinate system of the NIR tomography images. While this approach is practical and works reasonably well, it has some subjectivity associated with it as well as problems associated with tissue deformation. Finally, as NIR tomography transitions into a tool for imaging patients with the goal of achieving faster

processing, a quantitative computational tool is necessary for consistent and efficient ROI detection and delineation to eliminate the use of subjective ROI detection. Further more, since evaluating a new imaging modality requires knowledge of the validity of the reconstructed images, this type of computational tool can be used to generate contrast-detail curves which can be used to objectively determine the system performance and allow accurate comparison to other imaging system.

To develop an accurate and efficient computational tool for automatically and efficiently segmenting out the ROI in a laboratory or clinical NIR tomography imaging system, an automated algorithm to calculate the contrast to noise ratio (CNR) is needed. Similar to the signal-to-noise ratio in digital signal processing theory, the CNR is defined as the relative difference between the ROI and the background region values of the property, divided by the average variation in the background [13-15]. Though there is only one choice for the signal per guess calculation, there are different choices for the background. Ideally speaking, the property distribution of the constructed image should be exactly the same as the real image whose background, or the regular tissues, are uniform and identical everywhere. It is reasonable to randomly choose ROI region within the whole image. However, the intrinsic diffusion characteristic of the light traveling in the tissue makes every spot of the reconstructed image dependent to other locations of the same image. We need to take this into account and find the best solution for calculating the background properties. In this study, three methods of choosing background were investigated and compared, as detailed in sections below.

Contrast-detail curve is an accurate and objective way to evaluate the spatial resolution of a medical image system, especially in CT and MRI. It indicates the transition from a detectable ROI to a statistically insignificant un-detectable ROI. Traditionally, contrast-detail curves are derived subjectively by human inspection. It is reasonable to expect some inter-inspector variability in the development of the curves. Given a threshold CNR, if we can accurately calculate the real CNR value of the reconstructed images, we are able to construct consistent contrast-detail curves.

2. THEORY AND METHODS

2.1 Image Reconstruction

NIRFAST (Near Infrared Frequency domain Absorption and Scatter Tomography) is a Finite Element Method based reconstruction algorithm and it produces 3D images of absorption and scatter from boundary measurements of light transport through tissue [3, 12, 16]. In this work, a circular geometry of 86mm in diameter was chosen for simulation studies.

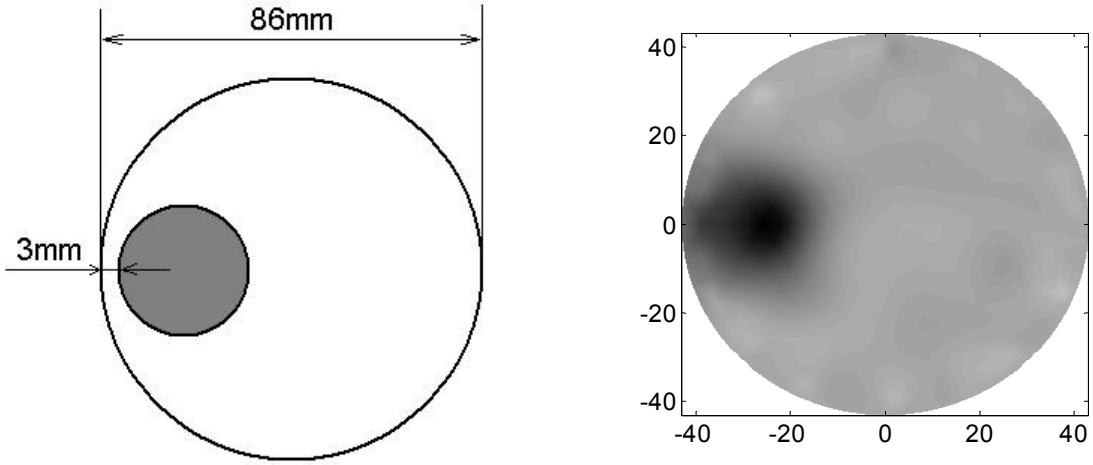

Figure 1. The geometry of the simulation optical property distribution is shown (left) and a typical absorption coefficient image that was reconstructed is shown (right) . This image was generated with simulated forward data using 1% noise in amplitude and 1^o noise phase shift using zero-mean Gaussian distributions.

The background has an absorption coefficient μ_a = 0.01mm^{-1}, and a reduced scattering coefficient μ_s' = 1.0 mm^{-1}. Within this field, a spherical heterogeneity of variable diameter was located 3mm away from the edge as depicted in Figure 1, with fixed μ_s' = 1mm^{-1} and a variable μ_a to provide the required contrast in absorption from 1.2:1 to 5.0:1. Forward calculations of diffusion theory were accomplished with a finite element numerical solution using a circular mesh with a set of regularly spaced node positions. Zero-mean Gaussian noise of 1% in amplitude and 1 degree in phase shift were added to calculated boundary data to simulate the realistic condition area in our NIR system. [16]

The image reconstruction process uses a Newton-Raphson approach to iteratively solve for the spatial distribution of optical properties, which minimizes the squared error between sets of measured (simulated) and calculated data. A Levenberg-Marquardt style regularization algorithm was used for stepping down the regularization parameter as the number of iterations progresses [16, 17]

2.2 Definitions of Contrast-to-Noise Ratio (CNR)

The matched filter technique [13-15] has been widely used for ultrasound imaging to detect the low-contrast target in a noisy background. Based on the description from the concept of the matched filter method [13], the background areas we first chose in the image field had the same radial-size and similar locations of the target, and they did not overlap with each other as described in Fig. 2(a), thus they had independent mean values and noises.

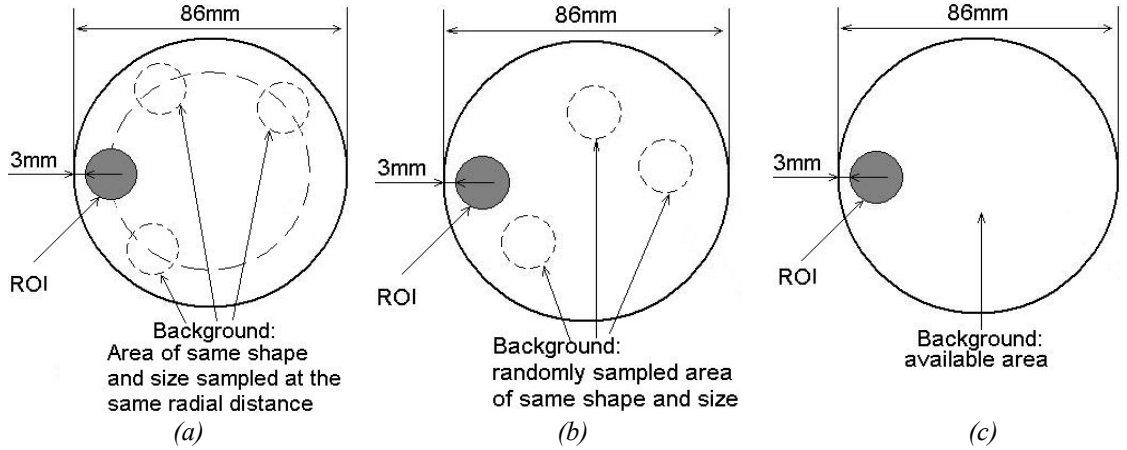

Figure 2. A schematic showing the three possible choices of backgrounds is shown including having it: (a) at the same radial location as the object, (b) randomly located, or (c) using the entire region outside of the target ROI.

We can define $\mu_{mean} = \frac{1}{n}\sum_{i=1}^{n}\mu_i$ as the mean value of the i_{th} background area in the whole image. If we define the contrast in reconstructed image as the relative difference of the mean values in the target and background, CNR could be defined as

$$CNR_I = \frac{contrast}{noise} = \frac{\Delta\mu}{noise} = \frac{\mu_{ROI} - \mu_{mean}}{\sqrt{(\sigma_{ROI}^2 + \sigma_{mean}^2)/2}} \quad (1)$$

Where ROI is referred to the suppositious target location with same shape and size as the real tumor and μ_{ROI} is the mean of the node values in the target, σ_{ROI} and σ_{mean} the standard deviations of the collectivities of the target and the mean of the background areas, respectively. Because the circular simulated target and background areas have the same size, it is reasonable to assume the target and background areas have the same noise weights.

However, the noise from the nodes that are closest to the field edge is higher because of the non-linear image reconstruction process here, and the fact that the weight functions (i.e. Jacobian matrices) have much higher

contributions nearest the source and detector locations. Overall, this contributes to higher system noise in regions nearest the edge of the field and lower values towards the center of the field. This effect is not accounted for in the above definition of CNR. In order to make sure that every node in the background has equal chance to contribute the background noise value, we introduce the second definition of CNR as

$$CNR_{II} = \frac{\mu_{ROI} - \mu_{random}}{\sqrt{(\sigma_{ROI}^2 + \sigma_{random}^2)/2}} \tag{2}$$

Where μ_{random} is the mean value of the nodes within a region having location that is randomly chosen in the variable background and σ_{random} is the standard deviation of these same nodes. While this definition has a good basis in statistical probability theory, the shortcoming of this definition is that the CNR depends on randomly picked nodes in the whole image therefore CNR is not exactly identical among different calculations.

We compare the values of the nodes in ROI all over the background as the CNR was defined as

$$CNR_{III} = \frac{\mu_{ROI} - \mu_{background}}{\sqrt{w_{ROI}\sigma_{ROI}^2 + w_{background}\sigma_{background}^2}} \tag{3}$$

Where $\mu_{background}$ is the mean value over the variable background, w_{ROI} and $w_{background}$ are the noise weights in the target and background, which depend on the size of the target in the image field. Thus, all nodes in the background have same weight of contribution to the background noise in equation (3).

2.3 Detection of Location and Size of ROI in the Reconstructed Image

Estimates of the locations of the ROI in the reconstructed images are necessary in our simulation and experiment studies. We used two methods to detect the location of ROI with different sizes and absorption contrasts. In the first method, we assumed that CNR should be the maximum when the suppositional region was at the location of ROI, as shown in Figure 3. In this method, we calculated CNR by the third method defined in equation (3), which includes all of the available background as the background area. However, this algorithm requires a significant period of time to complete the calculations for all possible locations and sizes of the ROI within the field. Thus, we introduced a 2D linear convolution method to detect the ROI. In this method, we created the ROI pattern, and draw the correlation image by convolving it with the reconstructed image, in which the highest correlation location corresponds to the maximum CNR, as depicted in Figure 4. Comparing this approach with the previous method, the advantage of the 2D linear convolution method is that it decreases the calculation time from several minutes to a few seconds for processing one image.

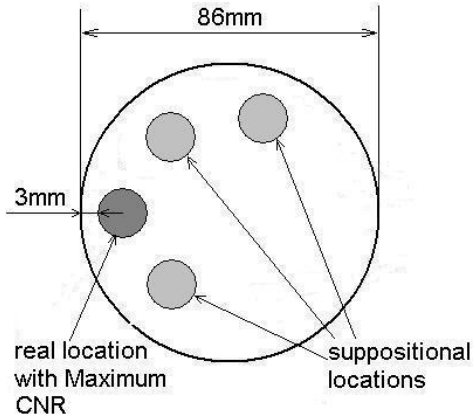

Fig. 3 Detection of the ROI by searching the maximum CNR from all of the suppositional locations in the image field is illustrated in this schematic, where suppositional locations are randomly tested and the sizes of these regions are

varied. This approach is used to determine when the CNR calculation is maximal, and yields an estimate of the size and location of the ROI, but requires a significant amount of computational time to achieve the result.

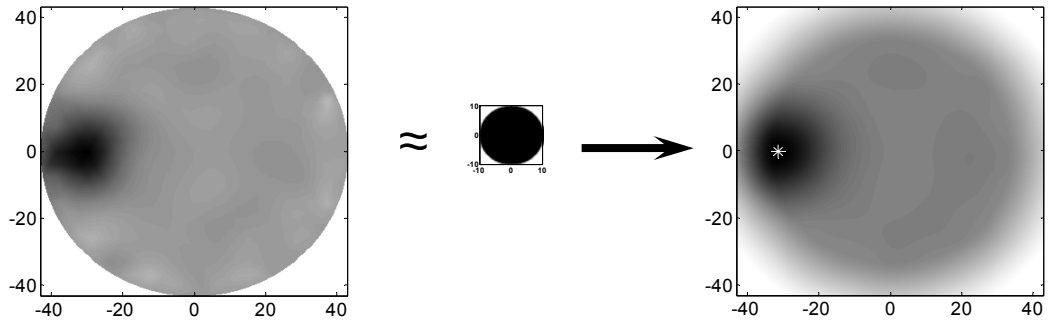

(a) *(b)* *(c)*

Fig. 4. The approach of using a 2D linear convolution is illustrated here where the 2D image shown in (a) is convolved with one test diameter ROI (b), and the resulting image shown in (c) is directly proportional to a CNR value plot. In the correlation image the highest value is marked with a small star (in (c)) which approximately defines the center of the ROI

Finally, if either the location or the size of the ROI in a reconstructed image is unknown, we could detect the ROI location by repeating this calculation through a series of the sizes for the test ROI. This approach is discussed in the next section with respect to using the calculation to define the true size of the ROI.

3. RESULTS

3.1 Evaluating the three methods of calculating CNR

Assuming that the real diameter and location of the target are given, we calculated CNR by using the three methods described in previous section as the absorption contrast and the ROI size were systematically varied. Figure 5 shows the difference of the CNR values of three methods. As shown in Figure 6, both the target with a larger size (23mm diameter) and low contrast (1.4 in absorption) and the targets with smaller size (3mm diameter) having high contrast (3.8 in absorption) can be observed in the reconstructed images if the CNR is greater than 4 for all of the three calculation methods. Thus, it is reasonable to set CNR = 4 as the detection threshold, although clearly a fuller study of what CNR corresponds to that used by humans should be carried out. Nonetheless, CNR=4 was used as a possible threshold throughout this study. The actual CNR values are plotted for all sizes and absorption contrast, as shown in Figure 5 (a, b, c), as well as the system contrast-detail curve Figure 5 (c) assuming a decision threshold of CNR = 4.

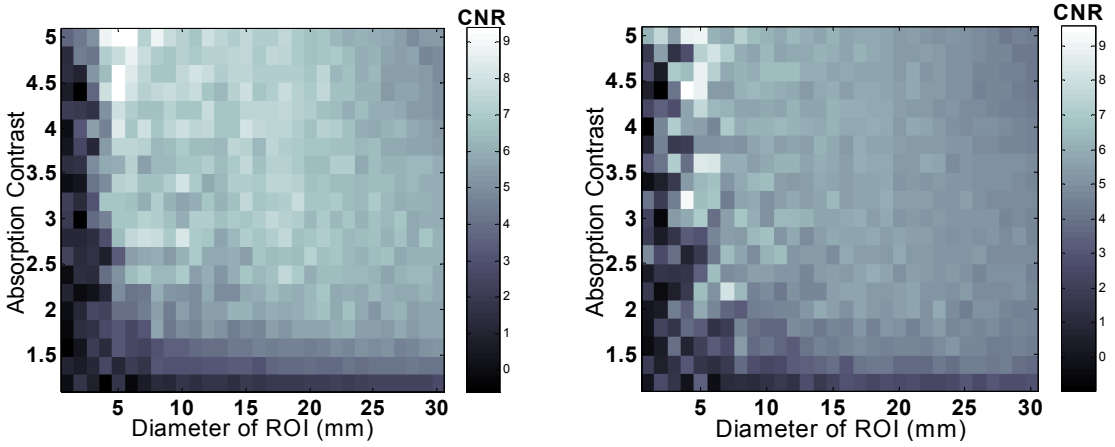

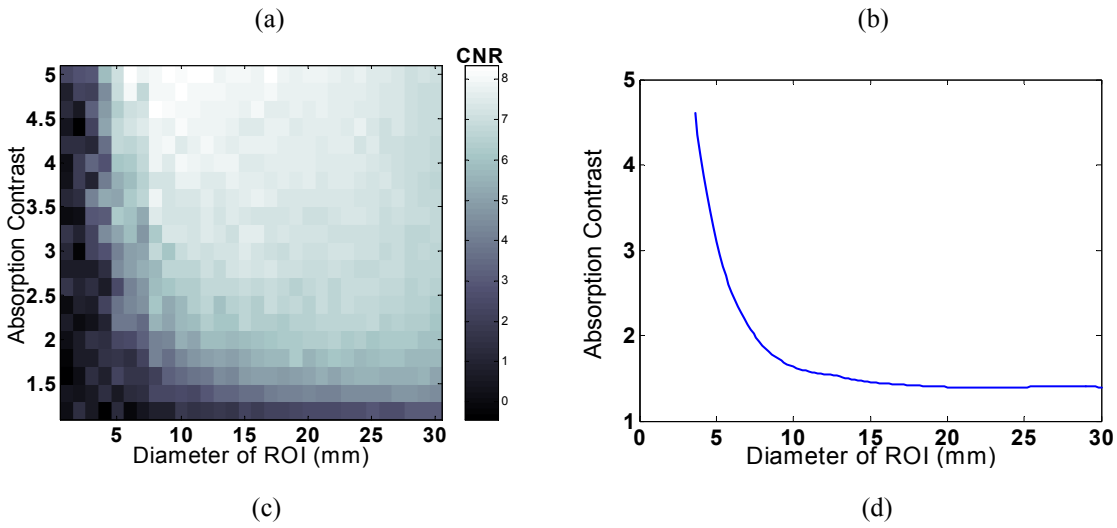

Fig. 5. Graphs of CNR distribution (color bar scale is CNR) are shown using the three different methods of choosing the background areas including (a) ROI sampled at the same radial distance in the image, (b) randomly sampled ROI of the same size as the original and (c) using all of the available background. Based on the last method shown in (c),the exact values of size and contrast were determined from (c) and the contrast-detail curve for these images are shown plotted in (d) using detection threshold of CNR = 4.

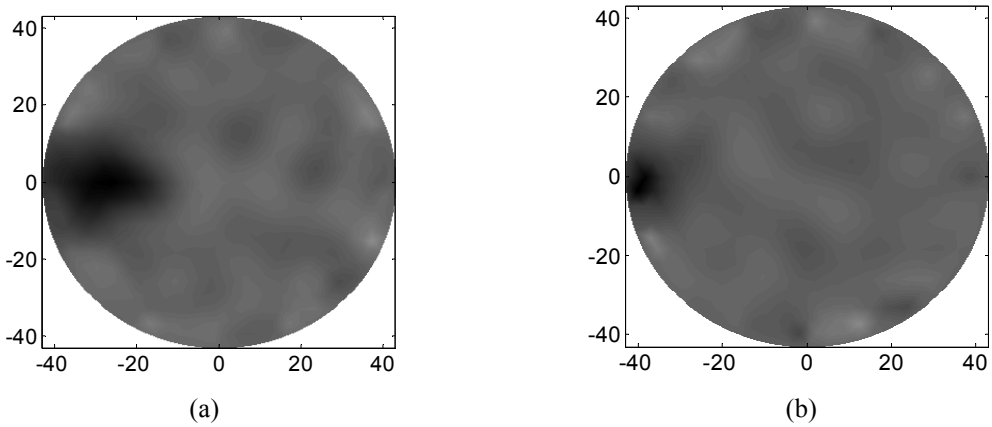

Fig. 6: Absorption reconstructed images as (a) the target with the large size (23mm diameter) and low contrast (1.4) and (b) the target with the small size (3mm diameter) and high contrast (3.8), in which CNR is great than 4 by all of three calculation method.

3.2 Detection of the location of ROI

From the previous part of this paper, we used both the node-by-node method, in which the maximum CNR from all of the suppositional regions in the image field is searched, and the 2D linear convolution method, in which the maximum correlation location between the ROI pattern and the reconstructed image profile was detected. In both methods the CNR was calculated by Equation (3) and the differences between the true location of ROI and its detected location were compared at different contrast values, as shown in Figure 7.

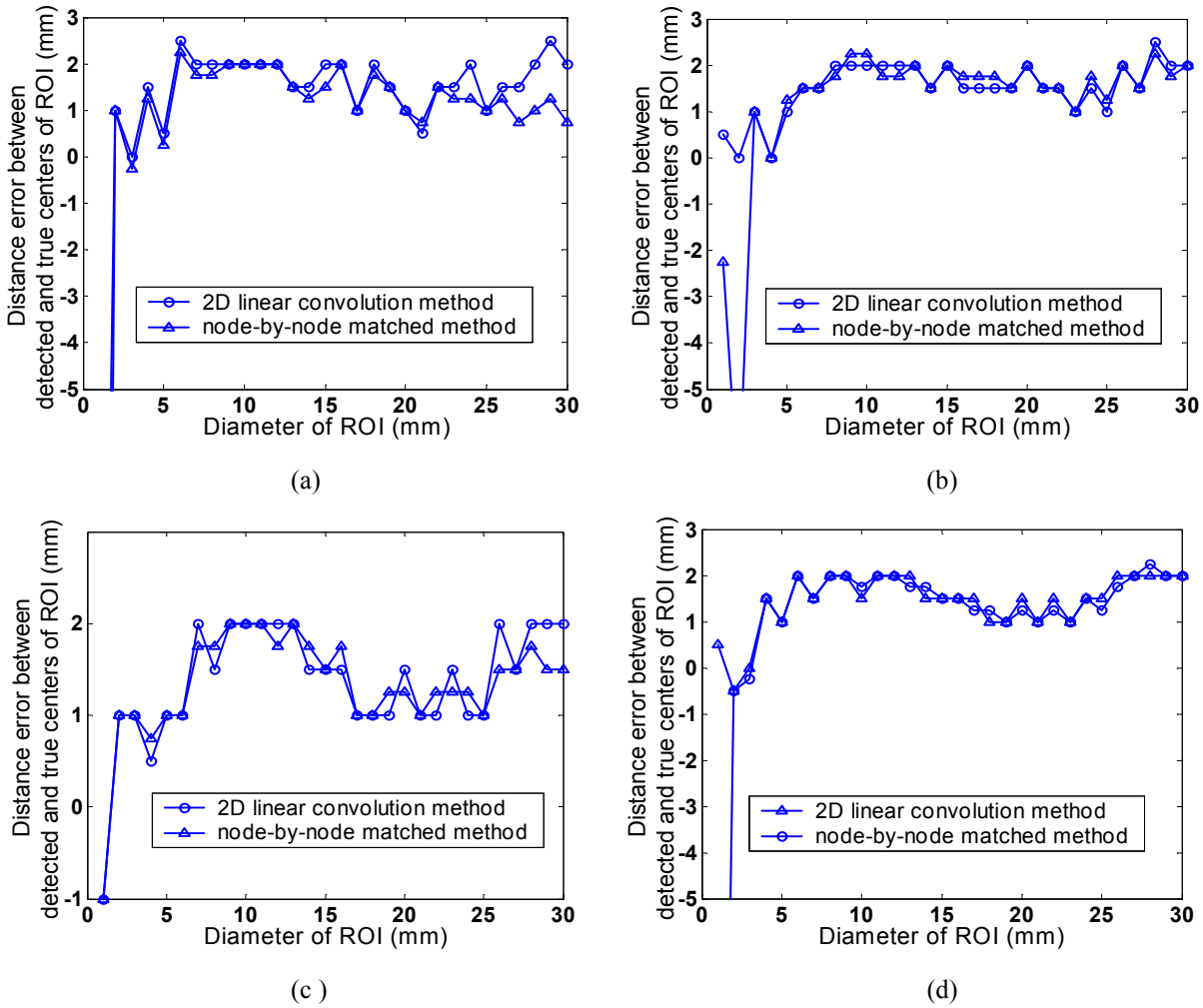

Fig. 7: The distance error between the detected center of ROI in the reconstructed imaging relative to the real location of spherical ROI center is plotted as a function of the diameter of ROI using absorption contrast values of (a) 2.0, (b) 3.0, (c) 4.0 and (d) 5.0, in the target relative to the background.

Figure 7 shows that the error between the detected and true locations of the ROI is even larger than the size of the ROI in both detection methods if the diameter of the target is less than 3mm and the contrast is low (i.e. equal to 2 in (a)). As the contrast increases (b, c, d), the location error from the node-by-node matching method is less than 1mm, but it requires a maximum CNR much lower than 4, the CNR threshold we assumed in the former section. Meanwhile, the error from the 2D linear convolution method is also very large when the diameter of ROI is small. Thus, neither of the two detection methods can find the location of the ROI if the diameter of heterogeneity is less than 3mm. As the diameter of the ROI becomes greater than 4mm, the location errors from both of the methods are around 1-2mm. Although the location error from the convolution method is slightly larger, it is more than 10 times faster.

3.3 Relationship between the tested and true diameter of ROI

Using the 2D linear convolution method, we studied the effect of changing the size of the heterogeneity region relative to the tested size of the ROI to see the relationship between the true and tested diameters. The values of CNR were plotted as a function of the tested diameter of ROI in Figure 8. Figure 8(a) shows that the curve of CNR values decreasing as the tested diameter of the heterogeneity increases, when the true region size is 5mm-diameter. When the real size of the target is equal to 7mm (b), CNR with high contrast (i.e. contrast greater than or equal to 3)

increased first as the tested diameter increased until the tested diameter was equal 4mm. This peak occurs at a region size which is 3 mm less than the true object diameter, and CNR reaches its maximum value. As the true diameter of the target keeps on increasing to be equal 10mm (c), the maximum CNR is at the tested diameter of ROI is equal to 7 mm, which is also 3 mm less than the true diameter. When the true diameter of the object increased to 15 mm, shown in (d), the CNR reached a maximum when the tested ROI diameter was 12 mm, for the condition where the contrast was not very high (i.e. less than or equal to 4).

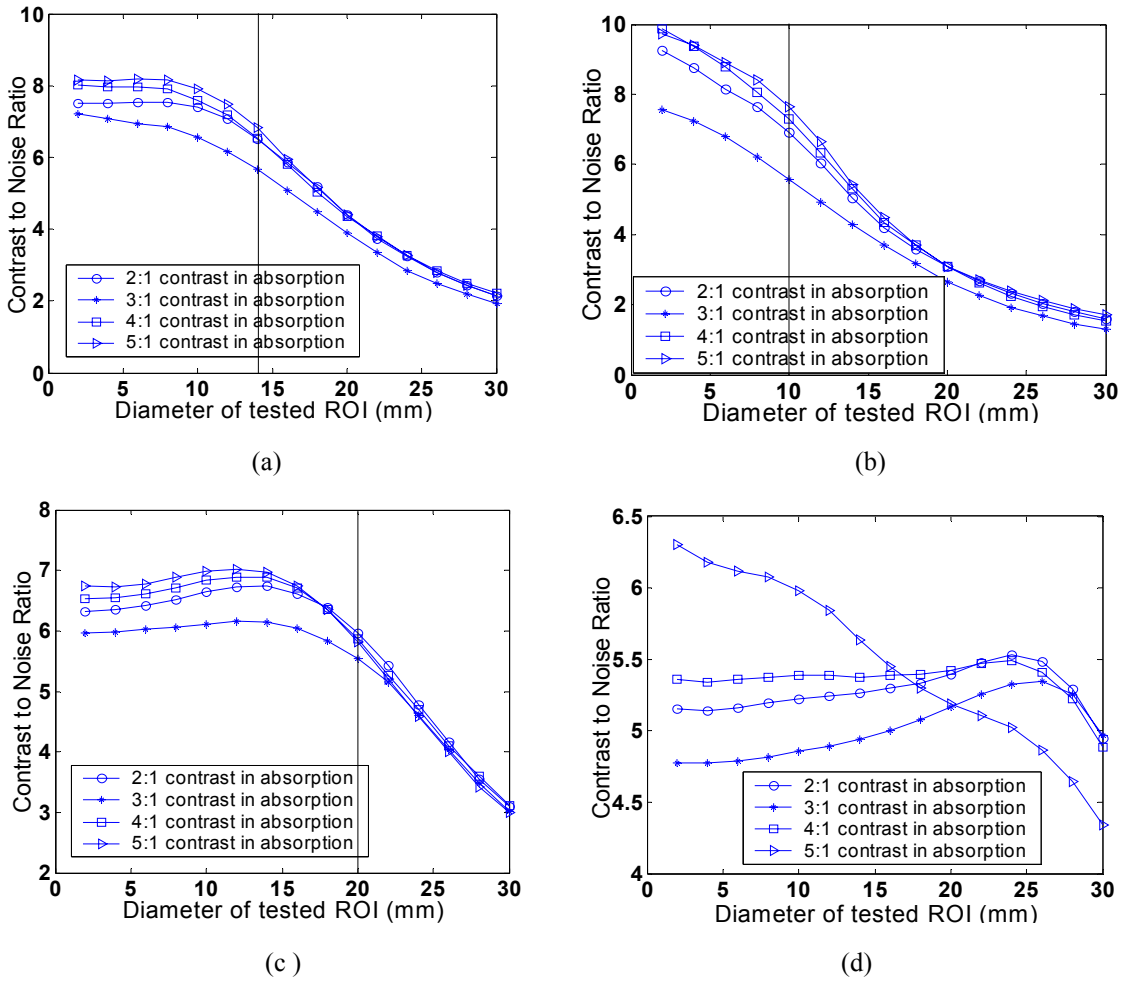

Fig. 8: Maximum CNR as a function of the test diameter of ROI at different absorption contrasts when the real diameter of ROI are (a) 10mm, (b) 14mm, (c) 20mm and (d) 30 mm. The vertical black solid line presents the real diameter of ROI in each graph.

4. DISCUSSION

4.1 Comparison with the different calculations of CNR

Comparing the three methods of calculating CNR, the resulting graphs in Figure 5 illustrate that the choice of background value can significantly impact our decision criteria of whether the region is "detected:" or not. The first definition that was based on the matched filter method in ultrasound imaging did not include the information about the nodes closed to the edge of the image field. This contributed to a higher noise because of the impact of the spatially dependent noise in NIR tomographic images, where most high frequency noise is located in the periphery of the image. The second method for calculation of CNR picked the background nodes randomly in the image field thus all of the nodes in the background had the same chance to be sampled, but it was not stable when the target is

very small. Finally, the last method of calculating CNR appeared to be the best, as it included all of the nodes in the background image and corrected the noises weights based on the size ratio of ROI and whole image field.

Based on the Fig 5(c) from the third method, we draw Fig. 5(d), where the blue regions represent the undetectable conditions and the red regions represents the detectable conditions, assuming the CNR threshold is 4. From Figure 5(c), the spatial resolution of our imaging system is 4mm diameter when the contrast is high (i.e. greater than or equal to a contrast of 4.4); and the contrast resolution is 1.4 as the diameter of the target is large (i.e. greater than or equal to 17mm) with 1% zero-mean Gaussian noise and 1^{o} phase shift added.

4.2 Detection of the location of ROI

As shown in Figure 8, the node-by-node matched and 2D linear convolution methods have very similar results for detection of the ROI location in the reconstructed image. Neither of the two methods were able to detect the ROI location when the diameter of the object being imaged was less than 3mm. While the diameter of the target increases, the reconstruct positional error range was around 1-2 mm toward to the field edge. Meanwhile, the location errors have no obvious change as the absorption contrast changes from 1.4 (the contrast resolution of our imaging system) to 5 if the diameter is the same. However, we consider the 2D linear convolution method is optimal for the purposes of our system, mainly because it is significantly faster, especially when the size of the target is small.

4.3 Relationship between the tested and true diameters of ROI

If the true diameter of the object is less than 6mm, the value of CNR will decreases as the tested diameter increases. As the real size of the heterogeneity increases to the 7 to 14mm range, the maximum CNR occurs at the place where the tested diameter of ROI is 3mm less than the true object diameter. At this same condition, the larger the contrast is the higher the value of CNR will be. If the true diameter of the ROI is greater than 15mm, the CNR value still reaches the maximum when the tested diameter of ROI is 3mm less if the contrast is low (i.e. less than or equal to 4).

5. CONCLUSIONS

In this simulation study, we calculated CNR by choosing the background areas included (i) ROIs sampled at the same radial distance in the image (ii) randomly sampled ROI of the same size as the original, and (iii) all of the available background. According to the comparing study the third method appears to be optimal for NIR tomography because it includes the nodes closest to the filed edge. This approach contributed higher background noise and is more stable than the other two methods, especially when the target is small. Based on the CNR defined by the third calculation method and a system decision threshold of CNR = 4, we find the NIR imaging system spatial resolution is 4mm-diamter and the contrast resolution is 1.4.

Two approaches were tested to find the location and size of the object based upon maximal CNR, including a random node-by-node matching process and a 2D linear convolution method. Although the results from these two methods are very similar, the convolution method is faster than the other one.

Finally, we used the convolution method to detect the size of target by changing the diameter of the tested ROI pattern. The true diameter of the target is consistently 3 mm larger than the tested diameter, where the location detection was based upon the value of CNR which was maximal. However, this approach will likely only be viable if the size of the target is greater than 7 mm in diameter and has higher contrast values is between 2 and 5.

In the future we plan to conduct similar studies to experimental data acquired on phantoms with a prototype imaging system intended for characterizing breast tissue and integrate this tool set into the system. Furthermore, since only single anomaly was used in this study, we would like to upgrade this tool set to diagnose tissue with multiple anomalies. It is also useful to investigate simulated or experimental objects with highly heterogeneous background.

6. ACKNOWLEDGEMENTS

This work has been sponsored by the National Institutes of Health through grants PO1CA80139 and RO1CA69544.

7. REFERENCES

1. B.W. Pogue, C. Willscher, T. McBride, U.Osterberg and K. Paulsen, *Contrast-detail analysis for detection and characterization with near-infrared diffuse tomography*, Med, Phys., vol. 27, no. 12, pp. 2693-2700, 2000
2. T. McBride, B. Pogue, S. Jiang, U. Osterberg, K. Paulsen and S. Poplack, *Initial studies of in vivo absorbing and scattering heterogeneity in near-infrared tomographic breast imaging*, Opt. Lett., vol. 26, no. 11, pp.822-824, 2001
3. B. W. Pogue, T. McBride, J. Prewitt, U. Osterberg and K. Paulsen, *Spatially variant regularization improves diffuse optical tomography*,, Appl. Opt., vol.38, no. 13, pp. 2950-2961, 1999.
4. J. C. Hebden, H. Veenstra, H. Dehghani, E. M. C. Hillman, M.Schweiger, S. R. Arridge, and D. T. Delpy, *Three dimensional time-resolved optical tomography of a conical breast phantom*, Appl. Opt. 40, 3278–3287, 2001
5. S. R. Arridge, *Topical review: optical tomography in medical imaging*, Inverse Probl. 15, R41–R93, 1999
6. H. Eda, I. Oda, Y. Ito, Y. Wada, Y. Oikawa, Y. Tsunazawa, Y. Tsuchiya, Y. Yamashita, M. Oda, A. Sassaroli, Y. Yamada, and M. Tamaru, *Multichannel time-resolved optical tomographic imaging system*, Rev. Sci. Instrum. 70, 3595–3602, 1999
7. D. A. Boas, D. H. Brooks, E. L. Miller, C. A. DiMarzio, M. Kilmer, R. J. Gaudette, and Q. Zhang, *Imaging the body with diffuse optical tomography*, IEEE Signal Proc. Mag. 18, 57–75, 2001
8. E. M. C. Hillman, J. C. Hebden, M. Schweiger, H. Dehghani, F. E. W. Schmidt, D. T. Delpy, and S. R. Arridge, *Time resolved optical tomography of the human forearm*, Phys. Med. Biol. 46, 1117–1130, 2001
9. S. Fantini, M. A. Franceschini, E. Gratton, D. Hueber, W.Rosenfeld, D. Maulik, P. G. Stubblefield, and M. R. Stankovic, *Non-invasive optical mapping of the piglet in real time*, Opt. Express 4, 308–314, 1999
10. V. Ntziachristos, A. H. Hielscher, A. G. Yodh, and B. Chance, *Diffuse optical tomography of highly heterogeneous media*, IEEE Trans. Med. Imaging 20, 470–478, 2001
11. H. B. Jiang, K. D. Paulsen, U. L. Osterberg, and M. S. Patterson, *Frequency-domain optical image reconstruction in turbid media: an experimental study of single-target detect ability*, Appl. Opt. 36, 52–63, 1997
12. T. O. McBride, B. W. Pogue, U. L. Osterberg, and K. D. Paulsen, *Image reconstruction of continuously varying objects and simulated breast cancer lesions*, in Optical Tomography and Spectroscopy of Tissue III, B. Chance, R. Alfano, and B. Tromberg, eds., Proc. SPIE 3597, 514–525, 1999
13. R. F. Wagner, S. W. Smith, J. M. Sandrik and H. Lopez, *statistics of speckle in ultrasound B-scans*, IEEE Trans. Sonics Ultrasound; SU-30:156-163, 1983
14. J. J. Rownd, E. L. Madsen, J. A. Zagzebski, G. R. Frank and F. Dong, *Phantoms and automated system for testing the resolution of ultrasound scanners*, Ultrasound in Med. & Biol. Vol. 23, No. 2, pp. 245-260, 1997
15. H. Lopez, M. H. Loew and D. J. Goodenough, *Objective analysis of ultrasound images by use of a computational observer*. IEEE Trans. Med. Imaging vol. 11, no. 4, pp. 496-506, 1992
16. B. W. Pogue, X. Song, T. D. Tosteson, T. O. McBride, S. Jiang, K. D. Paulsen, *Statistical Analysis of Non-linearly Reconstructed Near-Infrared Tomographic Images: Part I - Theory and Simulations*, IEEE Trans. Med. Imaging 21, 755-763, 2001
17. X. Song, B. W. Pogue, T. D. Tosteson, T. O. McBride, S. Jiang, K. D. Paulsen, *Statistical Analysis of Non-linearly Reconstructed Near-Infrared Tomographic Images: Part II – Experimental Interpretation*, IEEE Trans. Med. Imaging 21, 764-772, 2001